Article ID: 1000-324X(2021)12-1337-06 **DOI:** 10.15541/jim20210177

Sn Quantum Dots for Electrocatalytic Reduction of CO_2 to HCOOH

TIAN Jianjian[1,2], MA Xia[1,2], WANG Min[1], YAO Heliang[1], HUA Zile[1], ZHANG Lingxia[1,2,3]

(1. State Key Laboratory of High Performance Ceramics and Superfine Microstructure, Shanghai Institute of Ceramics, Chinese Academy of Sciences, Shanghai 200050, China; 2. Center of Materials Science and Optoelectronics Engineering, University of Chinese Academy of Sciences, Beijing 100049, China; 3. School of Chemistry and Materials Science, Hangzhou Institute for Advanced Study, University of Chinese Academy of Sciences, Hangzhou 310024, China)

Abstract: Sn based materials, as low-cost and earth-abundant electrocatalysts, are potential candidates for CO_2 reduction reaction (CO_2RR) into liquid fuels. Unfortunately, the low selectivity and stability limits their applications. Herein, we developed an electrocatalyst of Sn quantum dots (Sn-QDs) for efficient, durable and highly selective CO_2 reduction to HCOOH. The Sn-QDs were confirmed with high crystallinity and an average size of only 2–3 nm. Small particle size endowed the electrocatalyst with improved electrochemical active surface area (ECSA), which was about 4.4 times of that of Sn particle. This enlarged ECSA as well as accelerated CO_2RR kinetics favored the electrochemical conversion of CO_2. The Faradaic efficiency of HCOOH (FE_{HCOOH}) on Sn-QDs/CN reached up to 95% at –1.0 V (*vs* RHE), which exceeded 83% in the recorded wide potential window of 0.5 V. Moreover, the Sn-QDs electrocatalyst exhibited good electrochemical durability for 24 h.

Key words: CO_2 reduction; Sn quantum dots; HCOOH; electrocatalyst

With the increase of atmospheric CO_2 concentration, many eco-environmental problems are increasingly serious. Global endeavors are taken to capture and store or convert/utilize CO_2, in order to achieve zero carbon emission in future[1]. Electrocatalytic CO_2 reduction reaction (CO_2RR) receives extensive concern, because it can be operated under ambient pressure/temperature and is possible for scale-up industrialization[2]. CO_2 molecules can be converted into highly value-added carbon-containing products by sustainable electricity[3]. However, multiple proton and electron transfer steps involved in CO_2RR are kinetically sluggish, resulting in high overpotential or low Faradaic efficiency[1,4]. Therefore, it is urgent to develop highly efficient electrocatalysts to reduce CO_2 into target products with high selectivity at low overpotentials.

The pathways of CO_2RR involve successive CO_2 adsorption and activation, intermediate formation and conversion, finally products desorption from electrocatalyst surface[5]. Previous publications elucidated that the catalytic activity and production selectivity of metallic catalysts have a striking relation with their particle size, as the electronic structure and the adsorption of intermediates always vary according to particle size[6-11]. Generally, with the size decrease of metallic catalyst, the electrochemical active surface area (ECSA) and the number of active sites on its surface for CO_2RR increases. Likewise, in a certain size range, the activity of metallic catalyst and the Faradaic efficiency (FE) of products increase as the size of metallic catalyst decreases[6,12]. For example, Gu's group[11] found out variance in size effect of Ni metal on CO_2RR performance. Ni single atoms exhibited superior CO_2RR activity with FE_{CO} of 97%. While, for Ni particles, the FE_{CO} slightly lowered to 93% at the particle size of 4.1 nm and even decreased to below 30% accompanied with FE_{H2} of above 70% at the particle size of 37.2 nm.

Quantum dots (QDs) are desirable electrocatalysts for CO_2RR owing to their extra-small size, high dispersity and unique electronic properties[13-15]. For instance, N-doped graphene quantum dots (NG-QDs) achieved high CO_2 electro-reduction activity with high current density at low overpotentials. The increased pyridinic N species at edges were recognized as active sites, and the

Received date: 2021-03-19; **Revised date:** 2021-05-07; **Published online:** 2021-05-25
Foundation item: National Key R&D Program of China (2017YFE0127400); National Natural Science Foundation of China (51872317, 21835007); Science and Technology Commission of Shanghai (20520711900)
Biography: TIAN Jianjian (1989–), female, PhD. E-mail: tianshujian11@163.com
田建建(1989–), 女, 博士. E-mail: tianshujian11@163.com
Corresponding author: ZHANG Lingxia, professor. E-mail: zhlingxia@mail.sic.ac.cn
张玲霞, 研究员. E-mail: zhlingxia@mail.sic.ac.cn

decreased size of NG-QDs brought fastened kinetics[15]. Metal QDs catalysts (Pb, Au, Ag QDs as well as Cu QDs) derived from metal chalcogenide QDs exhibited drastically enhanced CO_2RR performances partially resulting from the increased propensity of CO_2 adsorption onto their surface[14]. The experiments and DFT calculations demonstrated that maximizing the atomic defects density in QDs favoured the localization of atomic and electronic structure, and lowered the energy barrier of CO_2RR. Inspired by these results, it is rational to design metallic catalysts with small size for improved CO_2RR performance. Herein, we synthesized Sn-QDs for CO_2RR to produce HCOOH *via* an *in-situ* electrochemical reduction process.

1 Experimental section

Sn particle decorated polymeric carbon nitride, denoted as Sn-p/CN, was prepared according to our previous work[16]. Sn quantum dots decorated polymeric carbon nitride, named as Sn-QDs/CN, was obtained *via* an *in-situ* electrochemical reduction process on Sn-p/CN in a three-electrode system. Typically, 20.0 mg of the as-prepared Sn-p/CN was dispersed in 2 mL of isopropanol and 80 μL of Nafion solution (weight percentage: 5%) under sonication for 1 h. Then, 20 μL of the ink was dropped onto the surface of the glassy carbon electrode with a diameter of 0.5 cm. To ensure Sn-p/CN was totally converted to Sn-QDs/CN, the electrode was *in-situ* reduced at –1.51 V (*vs*. Ag/AgCl) in CO_2-saturated 0.1 mol·L^{-1} $KHCO_3$ solution for 2 h. The as-obtained Sn-QDs/CN electrode was washed with water several times and immersed in electrolyte immediately, then was used as the working electrode for the follow-up measurements of electrochemical CO_2RR. The small amount of Sn-QDs/CN was scraped from the glassy carbon electrode and washed with water for further characterizations.

2 Results and discussion

As described in the experimental section, Sn-QDs/CN was synthesized by an *in-situ* electro-chemical-reduction process, similarly to the previously mentioned methods in the literatures[17-18]. The crystal structure of the as-synthesized Sn-QDs/CN sample was characterized by XRD, as shown in Fig. 1. The weak peak at 2θ=~27.9° corresponds to the (002) interlayer reflection of the graphitic-like structure of CN[19-20]. The other peaks at 2θ=30.6°, 32.0°, 43.9° and 44.9° are assigned to the (200), (101), (220) and (211) planes of tetragonal Sn (JCPDS 04-0673).

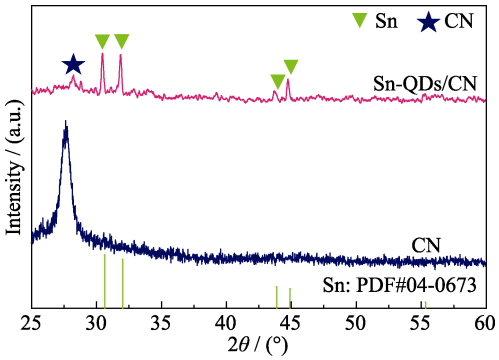

Fig. 1 XRD patterns of Sn-QDs/CN and CN

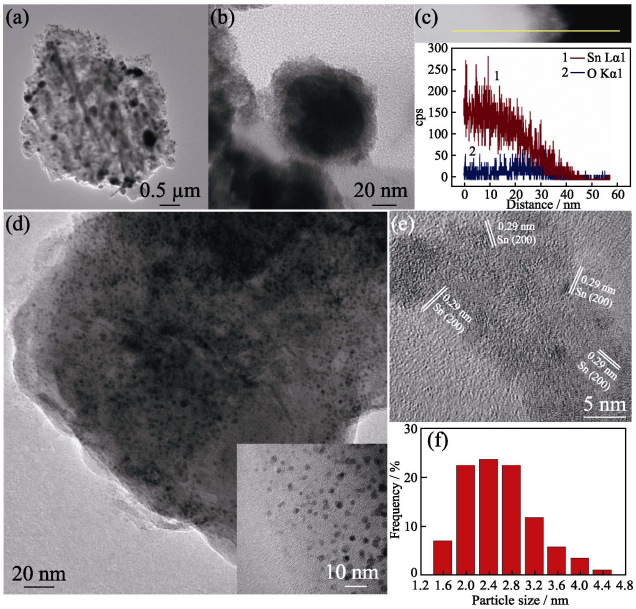

Fig. 2 TEM images at different magnifications (a, b) and corresponding EDS line scanning spectra (c) of Sn-p/CN; TEM image (inset: magnified image) (d), HRTEM image (e) and Sn-QDs size distribution (f) of Sn-QDs/CN

The TEM images of Sn-p/CN in Fig. 2(a) show that Sn particles in arbitrary size (50–500 nm) are dispersed on the surface of CN. From the TEM image (Fig. 2(b)) and EDS line scanning spectra (Fig. 2(c)), a thin Sn oxide (SnO_x) layer (light regions) forms on the surface of metallic Sn particles (dark regions), due to the oxidation of Sn in air[21]. Compared to Sn-p/CN, the Sn-QDs are homogeneously dispersed on the surface of CN substrate (Fig. 2(d)). The size distribution histogram (Fig. 2(f)) shows that Sn-QDs possess a size range of 1.6–4.4 nm. Sn species in smaller size may expose more active sites for the enhanced performance of CO_2RR[11,22]. The highly magnified TEM image (Fig. 2(e)) reveals the good crystallinity of Sn-QDs, confirmed by the clear fringes with a lattice spacing of 0.29 nm, assigned to the (200) crystal plane of Sn (JCPDS 04-0673). On the bases of the above experimental results, Sn-QDs with an average size of only 2–3 nm was successfully decorated on CN

via an *in-situ* electro-chemical transformation from Sn-p/CN.

The surface chemical state of the Sn-QDs/CN electrocatalyst was investigated by XPS analysis. The high-resolution Sn3d XPS spectrum (Fig. 3(a)) shows that the surface of Sn-QDs/CN consists of both Sn^{4+} (495.4 and 487.0 eV) and Sn^0 (493.6 and 485.2 eV)[23]. In the O1s XPS spectrum (Fig. 3(b)), the two fitted O1s peaks at 530.6 and 533.6 eV, are assigned to O–Sn^{4+} and surface hydroxyl groups, respectively[24]. The existence of Sn^{4+} on the surface was inevitable because Sn-QDs/CN sample underwent reoxidation by exposure in air as it was transported to XPS[16]. The N1s XPS spectra (Fig. S2) can be deconvoluted into three peaks corresponding to the sp^2 hybridized N atoms (398.4 eV), tertiary N groups (399.7 eV) and amino groups (400.9 eV), similar with those of CN. Compared with CN, the content of –NH– increases from 6.8% of CN to 15.5% of Sn-QDs/CN, indicating the slight loss of tri-*s*-thiazine in CN substrate. The increased amine groups could enhance the chemical adsorption of CO_2 during CO_2RR[25].

As described at experimental section, once obtained by *in-situ* electrochemical-reduction, the Sn-QDs/CN electrode was investigated immediately to prevent its surface reoxidation. The CO_2RR performance of the Sn-QDs/CN catalyst was explored and summarized in Fig. 4. As shown in Fig. 4(a), a current density of about 0.6 mA·cm^{-2} is obtained at –1.0 V in Ar-saturated solution, which is ascribed to HER (Hydrogen evolution reaction). By comparison, in CO_2-saturated solution, the current density is ~2.0 mA·cm^{-2} at –1.0 V, which indicates that Sn-QDs/CN exhibits much higher CO_2RR activity than HER[26]. Fig. S3(a) shows that the current density of Sn-QDs/CN during CO_2RR increases with the rise of applied potentials, coinciding with the result of LSV in Fig. 4(a).

The Faradaic efficiencies of products at different applied potentials are plotted to evaluate the selectivity of the Sn-QDs/CN electrode (Fig. S3(b)). CO and HCOOH are generated in CO_2 electroreduction reaction. H_2 is produced from HER, the competing reaction with CO_2RR. On CN substrate (Fig. S4), no HCOOH is generated during CO_2RR, and H_2 is the major product. This signifies that the active sites of CO_2RR on Sn-QDs/CN are Sn-QDs. As revealed by Fig. S3(b), the Faradaic efficiency of HCOOH (FE_{HCOOH}) exceeds 83% in a record wide potential window of 0.5 V (from –0.8 V to –1.3 V), manifesting its high selectivity for HCOOH. To be specific, the Sn-QDs/CN electrode displays the maximum FE_{HCOOH} of around 95% at –1.0 V. While

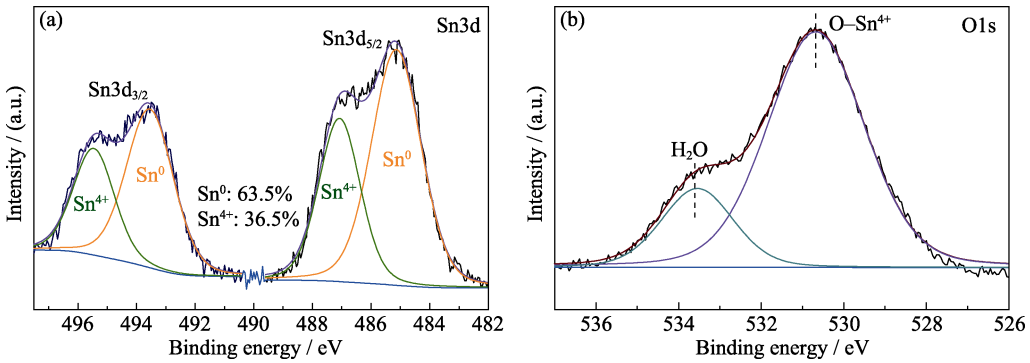

Fig. 3　High-resolution Sn3d (a) and O1s (b) XPS spectra of Sn-QDs/CN

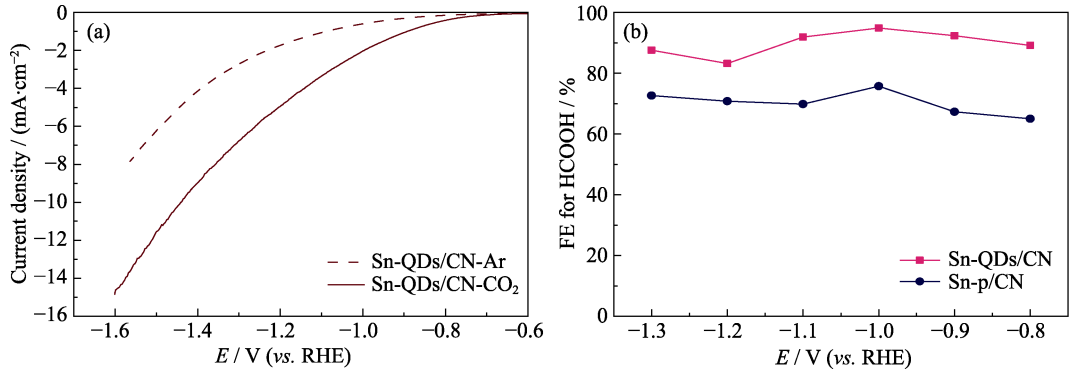

Fig. 4　LSV curves of the Sn-QDs/CN electrode in Ar-(dotted line) and CO_2-saturated (solid line) 0.1 mol·L^{-1} $KHCO_3$ electrolyte at a scan rate of 30 mV·s^{-1} (a), and Faradaic efficiencies of HCOOH on Sn-QDs/CN and Sn-p/CN at a series of potentials (b)

Sn-p/CN exhibits a maximum FE_{HCOOH} of only 75% at –1.0 V. Faradaic efficiencies of HCOOH on Sn-QDs/CN and Sn-p/CN are intuitively compared in Fig. 4(b) at a series of potentials. It can be observed clearly that Sn-QDs/CN shows much more outstanding CO_2RR performance for HCOOH production at all applied potentials. Therefore, it can be concluded that the performance of CO_2RR has a great relationship with the particle size. Moreover, the as-prepared Sn-QDs/CN electrode in CO_2-saturated 0.1 mol·L^{-1} $KHCO_3$ solution exhibits enhanced current density compared to Sn-p/CN in the examined potential range (Fig. S5), indicating that the catalytic activity on CO_2RR of Sn-QDs/CN is much higher than that on Sn-p/CN.

To explore the effect of particle size on the performance of CO_2 reduction, the double-layer capacitance was measured to estimate the ECSA of catalyst. As shown in Fig. 5(a), Sn-QDs/CN presents higher capacitance (0.053 mF·cm^{-2}) than Sn-p/CN (0.012 mF·cm^{-2}), which indicates that the ECSA of Sn-QDs/CN is about 4.4 times of that of Sn-p/CN. The increased ECSA means more active sites exposed for CO_2RR, contributing to the enhanced catalytic performance. Moreover, Sn-QDs/CN possesses a smaller radius of impedance than Sn-p/CN (Fig. 5(b)). It can be seen from Table S2 that the fitted charge transfer resistance (R_{ct}) of Sn-QDs/CN is 276.3 Ω, which is much smaller than that of Sn-p/CN (336.9 Ω). It manifests that the charge-transfer impedance in Sn-QDs/CN is much smaller than that in Sn-p/CN, i.e., much faster electron transfer in Sn-QDs/CN catalyst during CO_2RR[27].

To better explore the kinetic mechanism of CO_2RR, Tafel slope was further analysed. Tafel plots for HCOOH production are presented in Fig. 5(c). The measured Tafel slope values of Sn-QDs/CN and Sn-p/CN are 170 and 250 mV·dec^{-1}, respectively, which are both close to the theoretical value of 116 mV·dec^{-1}. The data imply that the rate-determining step (RDS) on these two catalysts for CO_2RR is supposed to be one electron transfer to CO_2 to form CO_2^- intermediate[28]. Besides, the lower Tafel slope of Sn-QDs/CN indicates its much faster CO_2RR kinetics than Sn-p/CN, consistent with the result of EIS.

Except for the high electrocatalytic performance for HCOOH production in CO_2RR, Sn-QDs/CN electrocatalyst also showed good electrochemical durability. In Fig. 5(d), it can be found that both FE_{HCOOH} and the current density display no obvious decay during the continuous CO_2RR at –1.0 V for 24 h. The electrochemical stability implies the favorably stable structure of Sn-QDs/CN.

3 Conclusion

In summary, we have successfully fabricated an electrocatalyst (Sn-QDs/CN) with Sn quantum dots (Sn-QDs)

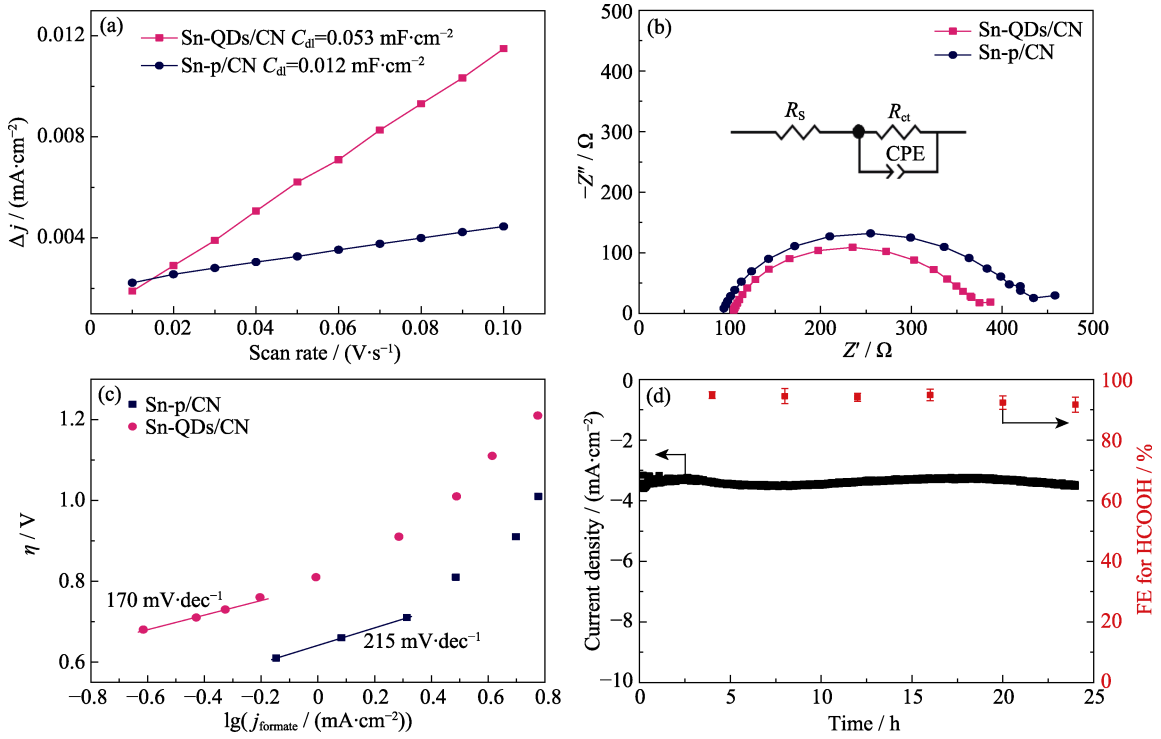

Fig. 5 Charging current density differences plotted against scan rates (a), electrochemical impedance spectra with inset showing the corresponding equivalent circuit (b), Tafel plots for HCOOH production on Sn-QDs/CN and Sn-p/CN (c), and the stability of Sn-QDs/CN catalyst at –1.0 V for 24 h in CO_2-saturated 0.1 mol·L^{-1} $KHCO_3$ (d)

decorated on polymeric carbon nitride (CN) by an *in-situ* electrochemical reduction process conducted on Sn particles loaded CN (Sn-p/CN) in a three-electrode system. The Sn-QDs with good crystallinity exhibit an average size of only 2–3 nm. The smaller size brings more active sites exposed, and the electrochemical active surface area (ECSA) of Sn-QDs/CN also increases by about 3.4 times in comparison with Sn-p/CN. The Faradic efficiency of HCOOH (FE_{HCOOH}) reached up to 95% on Sn-QDs/CN at –1.0 V and kept above 83% in a recorded wide potential window exceeding 0.5 V. Furthermore, the Sn-QDs/CN electrocatalyst also showed good electrochemical stability during the CO_2RR of 24 h. The advanced performance of Sn-QDs/CN can be attributed to the enlarged ECSA, fastened electron transfer and enhanced kinetics derived from the decreased particle size of Sn-QDs. This work provides a perspective to synthesize metal QDs electrocatalysts for highly efficient CO_2RR to HCOOH.

Supporting materials

Supporting materials related to this article can be found at https://doi.org/10.15541/jim20210177.

References:

[1] LI X D, WANG S M, LI L, *et al*. Progress and perspective for *in situ* studies of CO_2 reduction. *Journal of the American Chemical Society*, 2020, **142:** 9567–9581.

[2] BIRDJA Y Y, PEREZ-GALLENT E, FIGUEIREDO M, *et al*. Advances and challenges in understanding the electrocatalytic conversion of carbon dioxide to fuels. *Nature Energy*, 2019, **4:** 732–745.

[3] VASILEFF A, ZHENG Y, QIAO S Z. Carbon solving carbon's problems: recent progress of nanostructured carbon-based catalysts for the electrochemical reduction of CO_2. *Advanced Energy Materials*, 2017, **7(21):** 1700759.

[4] SHAO P, YI L C, CHEN S M, *et al*. Metal-organic frameworks for electrochemical reduction of carbon dioxide: the role of metal centers. *Journal of Energy Chemistry*, 2020, **40:** 156–170.

[5] ZHANG L, ZHAO Z J, GONG J. Nanostructured materials for heterogeneous electrocatalytic CO_2 reduction and their related reaction mechanisms. *Angewandte Chemie International Edition*, 2017, **56(38):** 11326–11353.

[6] MISTRY H, RESKE R, ZENG Z H, *et al*. Exceptional size-dependent activity enhancement in the electroreduction of CO_2 over Au nanoparticles. *Journal of the American Chemical Society*, 2014, **136(47):** 16473–16476.

[7] TYO E C, VAJDA S. Catalysis by clusters with precise numbers of atoms. *Nature Nanotechnology*, 2015, **10(7):** 577–588.

[8] GAO D F, ZHOU H, WANG J, *et al*. Size-dependent electrocatalytic reduction of CO_2 over Pd nanoparticles. *Journal of the American Chemical Society*, 2015, **137(13):** 4288–4291.

[9] LIU S G, HUANG S P. Size effects and active sites of Cu nano. particle catalysts for CO_2 electroreduction. *Applied Surface Science*, 2019, **475:** 20–27.

[10] LEE C H, KANAN M W. Controlling H^+ *vs* CO_2 reduction selectivity on Pb electrodes. *ACS Catalysis*, 2014, **5(1):** 465–469.

[11] LI Z D, HE D, YAN X X, *et al*. Size-dependent nickel-based electrocatalysts for selective CO_2 reduction. *Angewandte Chemie International Edition*, 2020, **59:** 2–8.

[12] RESKE R, MISTRY H, BEHAFARID F, *et al*. Particle size effects in the catalytic electroreduction of CO_2 on Cu nanoparticles. *Journal of the American Chemical Society*, 2014, **136(19):** 6978–6986.

[13] LÜ K L, SUO W Q, SHAO M D, *et al*. Nitrogen doped MoS_2 and nitrogen doped carbon dots composite catalyst for electroreduction CO_2 to CO with high Faradaic efficiency. *Nano Energy*, 2019, **63:** 103834.

[14] LIU M, LIU M X, WANG X M, *et al*. Quantum-dot-derived catalysts for CO_2 reduction reaction. *Joule*, 2019, **3(7):** 1703–1718.

[15] WU J J, MA S C, SUN J, *et al*. A metal-free electrocatalyst for carbon dioxide reduction to multi-carbon hydrocarbons and oxygenates. *Nature Communication*, 2016, **7:** 13869.

[16] TIAN J J, WANG M, SHEN M, *et al*. Highly efficient and selective CO_2 electro-reduction to HCOOH on Sn particle-decorated polymeric carbon nitride. *ChemSusChem*, 2020, **13(23):** 6442–6448.

[17] WEN G B, LEE D U, REN B H, *et al*. Orbital interactions in Bi-Sn bimetallic electrocatalysts for highly selective electrochemical CO_2 reduction toward formate production. *Advanced Energy Materials*, 2018, **8(31):** 1802427.

[18] LI P X, FU W Z, ZHUANG P Y, *et al*. Amorphous Sn/crystalline SnS_2 nanosheets *via in situ* electrochemical reduction methodology for highly efficient ambient N_2 fixation. *Small*, 2019, **15(40):** 1902535.

[19] TIAN J J, ZHANG L X, WANG M, *et al*. Remarkably enhanced H_2 evolution activity of oxidized graphitic carbon nitride by an extremely facile K_2CO_3-activation approach. *Applied Catalysis B: Environmental*, 2018, **232:** 322–329.

[20] WEN J, XIE J, CHEN X, *et al*. A review on g-C_3N_4-based photocatalysts. *Applied Surface Science*, 2017, **391:** 72–123.

[21] LAI Q, YUAN W Y, HUANG W J, *et al*. Sn/SnO_x electrode catalyst with mesoporous structure for efficient electroreduction of CO_2 to formate. *Applied Surface Science*, 2020, **508:** 145221.

[22] LIU S B, XIAO J, LU X F, *et al*. Efficient electrochemical reduction of CO_2 to HCOOH over Sub-2 nm SnO_2 quantum wires with exposed grain boundaries. *Angewandte Chemie International Edition*, 2019, **58:** 8499–8503.

[23] LUC W, COLLINS C, WANG S W, *et al*. Ag-Sn bimetallic catalyst with a core-shell structure for CO_2 reduction. *Journal of the American Chemical Society*, 2017, **139(5):** 1885–1893.

[24] BANG J H, CHOI M S, MIRZAEI A, *et al*. Selective NO_2 sensor based on Bi_2O_3 branched SnO_2 nanowires. *Sensors and Actuators B: Chemical*, 2018, **274:** 356–369.

[25] MA Y, WANG Z, XU X, *et al*. Review on porous nanomaterials for adsorption and photocatalytic conversion of CO_2. *Chinese Journal of Catalysis*, 2017, **38(12):** 1956–1969.

[26] CHEN Z, GAO M R, DUAN N, *et al*. Tuning adsorption strength of CO_2 and its intermediates on tin oxide-based electrocatalyst for efficient CO_2 reduction towards carbonaceous products. *Applied Catalysis B: Environmental*, 2020, **277:** 119252.

[27] NGUYEN T N, SALEHI M, LE Q, *et al*. Fundamentals of electrochemical CO_2 reduction on single-metal-atom catalysts. *ACS Catalysis*, 2020, **10(17):** 10068–10095.

[28] HE R, YUAN X, SHAO P F, *et al*. Hybridiztion of defective tin disulfide nanosheets and silver nanowires enables efficient electrochemical reduction of CO_2 into formate and syngas. *Small*, 2019, **15(50):** 1904882.

锡量子点制备及其电催化还原二氧化碳产甲酸性能

田建建[1,2], 马 霞[1,2], 王 敏[1], 姚鹤良[1], 华子乐[1], 张玲霞[1,2,3]

(1. 中国科学院 上海硅酸盐研究所, 高性能陶瓷和超微结构国家重点实验室, 上海 200050; 2. 中国科学院大学 材料科学与光电工程中心, 北京 100864; 3. 国科大杭州高等研究院 化学与材料科学学院, 杭州 310024)

摘 要: 锡基材料在自然界含量丰富、价格低廉, 在电催化还原 CO_2 制液体燃料反应中具有巨大潜力。但是较低的产物选择性和较差的稳定性限制了其应用。本工作制备的锡量子点电催化剂(Sn-QDs), 具有高效、高稳定性和高选择性的电催化还原 CO_2 产 HCOOH 活性。Sn-QDs 的平均颗粒尺寸仅为 2~3 nm, 结晶性良好。小的颗粒尺寸增大了电化学活性面积(ECSA), Sn-QDs 的 ECSA 约为锡颗粒的 4.4 倍。ECSA 增大以及 CO_2 还原反应动力学加速, 促进了 CO_2 电化学转化。在–1.0 V (*vs* RHE)下, Sn-QDs/CN 催化剂的 HCOOH 法拉第效率(FE_{HCOOH})达到 95%, 并且在宽约 0.5 V 的电势范围内能够保持在 83%以上。此外, Sn-QDs/CN 可以在 24 h 内保持良好的电化学稳定性。

关 键 词: CO_2 还原; 锡量子点; HCOOH; 电催化剂

中图分类号: TQ174 **文献标志码**: A

Supporting information:

Sn Quantum Dots for Electrocatalytic Reduction of CO_2 to HCOOH

TIAN Jianjian [1,2], MA Xia[1,2], WANG Min[1], YAO Heliang[1], HUA Zile[1], ZHANG Lingxia[1,2,3]

(1. State Key Laboratory of High Performance Ceramics and Superfine Microstructure, Shanghai Institute of Ceramics, Chinese Academy of Sciences, Shanghai 200050, China; 2. Center of Materials Science and Optoelectronics Engineering, University of Chinese Academy of Sciences, Beijing 100049, China; 3. School of Chemistry and Materials Science, Hangzhou Institute for Advanced Study, University of Chinese Academy of Sciences, Hangzhou 310024, China)

1 Characterizations

X-ray diffraction (XRD) patterns were acquired on a Rigaku D/ultima IV diffractometer (Cu Kα radiation). The X-ray photoelectron spectroscopy (XPS) measurement was conducted on a Thermo Scientific ESCAlab 250 spectrometers with Al Kα X-ray as radiation source, and the binding energies were calibrated using the C1s peak at 284.6 eV. The transmission electron microscope (TEM) and high resolution TEM (HRTEM) images were obtained on a JEM-2100F microscope.

2 Electrochemical measurements

All electrochemical measurements were performed in a gas-tight H-cell (separated by Nafion N117 membrane) connected to a Biologic VMP3 electrochemistry workstation. Each of cathodic and anodic compartments held 30 mL of electrolyte (CO_2-saturated 0.1 mol·L^{-1} $KHCO_3$) and 38 mL of headspace. The Pt mesh and Ag/AgCl electrode (with a saturated KCl solution) were used as the counter electrode and reference electrode, respectively. All measured potentials were converted to the reversible hydrogen electrode (RHE) without special illustration in the whole work. The linear sweep voltammetry (LSV) was recorded at a scan rate of 30 mV·s^{-1}. The current density was calculated by normalizing to the geometric surface area of the working electrode. Electrochemical impedance spectroscopy (EIS) measurement was carried out in the frequency range from 100 kHz to 10 Hz at –1.0 V (*vs* RHE). Double-layer capacitance (C_{dl}) was determined by measuring the capacitive current associated with double-layer charging from the scan-rate dependence of cyclic voltammogram (CV). The potential window of CV was 0 V to –0.1 V (*vs* RHE). The scan rates were 10–100 mV·s^{-1}. The C_{dl} was estimated by plotting the Δj ($\Delta j = j_a - j_c$) at –0.05 V (*vs* RHE) against the scan rates (j_a and j_c were the anodic and cathodic current densities, respectively). The slope was twice of that of C_{dl}.

Electrochemical CO_2 reduction was conducted at room temperature and atmospheric pressure. Prior to CO_2RR, high purity CO_2 gas (99.99%) was firstly purged into the cathodic compartment reservoir for 30 min to remove residual air, then the cathodic compartment was sealed. The anode chamber was open in order to vent out O_2 generated during the electrochemical test. The electrolyte in the cathode chamber was continuously stirred at a rate of 300 r·min^{-1} during the electrolysis to enhance the mass transport of CO_2. The CO_2RR was conducted for 2 h at each potential. The concentration of gaseous products was detected by gas chromatography (GC7900 Techcomp for H_2 and GC-2014 Shimadzu for CO). Liquid products were analyzed on a 500 MHz ^{1}H liquid NMR spectrometer (Bruker) with dimethyl sulfoxide (DMSO) as internal standard (Fig. S1(a)). The ^{1}H NMR spectrum was recorded using water suppression method. After electrolysis, the product-containing electrolyte (500 μL) was mixed with 100 μL of D_2O solution consisting of 12.46 mmol·L^{-1} DMSO for NMR test. The concentration of formate (HCOOH) was obtained based on the calibration curve (Fig. S1(b)). The Faradaic efficiency of the product was calculated as below: $FE_{product} = 2F \times n_{product}/Q$, where F is the Faraday constant (96485 C·mol^{-1}), n is the amount of production (mol), Q is the total charge consumed (C).

Table S1 Comparison of various Sn-based catalysts for CO_2-to-HCOOH conversion

Electrocatalyst	Electrolyte	Potential /V (*vs*. RHE)	FE_{HCOOH} /%	Current density /(mA·cm^{-2})	Stability/h	Ref.
Sn-QDs/CN	0.1 mol·L^{-1} $KHCO_3$	–1.0	95	3.3	24	This work
Sn quantum sheets confined in graphene	0.1 mol·L^{-1} $NaHCO_3$	–1.2	89	21.1	50	[1]
Nano-SnO_2/graphene	0.1 mol·L^{-1} $NaHCO_3$	–1.2	93.6	10	–	[2]
SnO_2 nanoparticles (< 5 nm)	0.1 mol·L^{-1} $KHCO_3$	–1.2	64	147	–	[3]

Continued

Electrocatalyst	Electrolyte	Potential /V (*vs*. RHE)	FE_{HCOOH} /%	Current density /(mA·cm^{-2})	Stability/h	Ref.
SnO_2 nanoparticles (~500 nm)	0.1 mol·L^{-1} $KHCO_3$	–1.2	83.5	7.56	–	[4]
SnO_2 nanoparticles (100 nm)	0.5 mol·L^{-1} $KHCO_3$	–0.9	80	12	–	[5]
SnO_2 nanoparticles (8–20 nm)	0.1 mol·L^{-1} $KHCO_3$	–1.06	82	15.3	5	[6]
SnO_2@N-CNW	0.5 mol·L^{-1} $NaHCO_3$	–0.8	90	13	20	[7]
SnO_2@N-rGO	0.5 mol·L^{-1} $NaHCO_3$	–0.8	89	21.3	20	[8]
SnO_2/PC	0.5 mol·L^{-1} $KHCO_3$	–0.86	92	29	10	[9]
SnO_2⊃NC@EEG	0.1 mol·L^{-1} $KHCO_3$	–1.2	81.2	13.4	10	[10]
SnO/C	0.5 mol·L^{-1} $KHCO_3$	–0.86	75	27.2	–	[11]

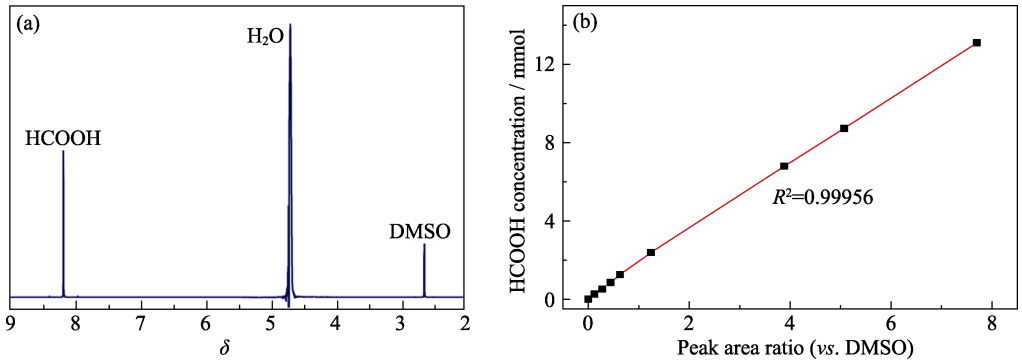

Fig. S1 ^{1}H NMR spectrum of the cathodic electrolyte after CO_2RR (a), and linear relationship between HCOOH concentration and relative peak area ratio (*vs*. DMSO) (b)

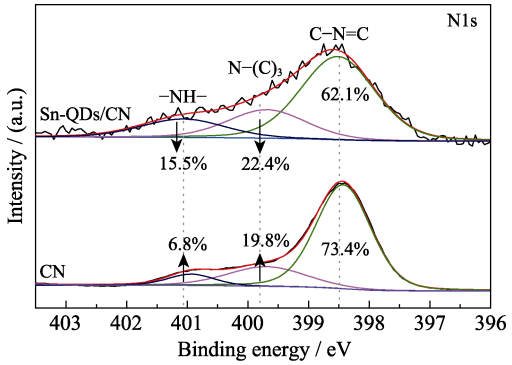

Fig. S2 High-resolution N1s XPS spectra of Sn-QDs and CN

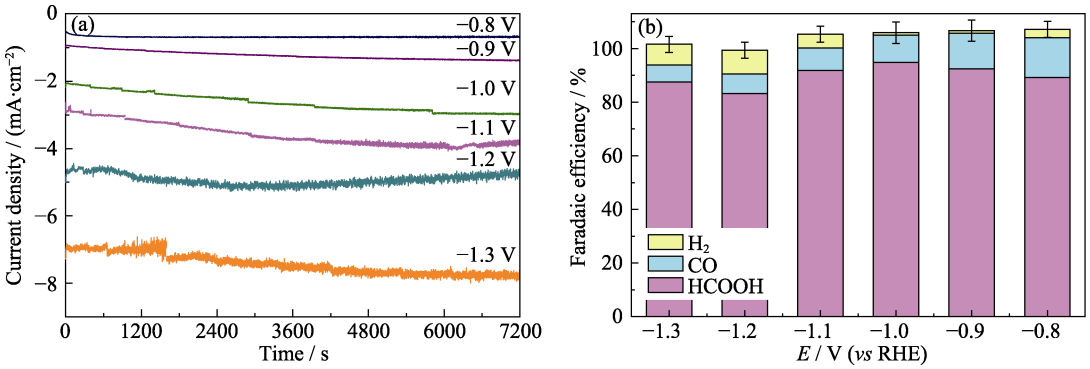

Fig. S3 *i-t* curves of CO_2RR on Sn-QDs/CN at different applied potentials (a), and Faradaic efficiencies of HCOOH, CO and H_2 at different applied potentials on the Sn-QDs/CN electrode (b)

Table S2　Fitted data of EIS for Sn-QDs/CN and Sn-p/CN

Parameter	R_s/Ω	R_{ct}/Ω	CPE-T	CPE-P
Sn-QDs/CN	102.6	276.3	1.2×10^{-5}	0.85
Sn-p/CN	96.74	336.9	1.1×10^{-5}	0.89

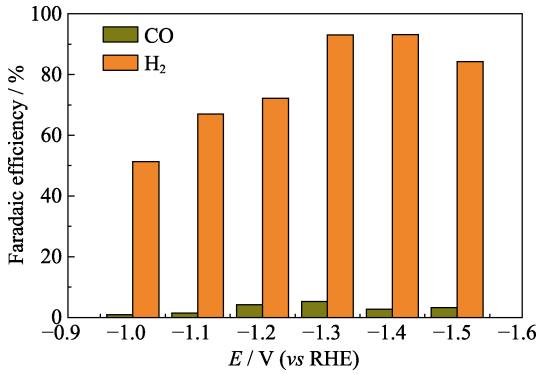

Fig. S4　Faradaic efficiencies of CO and H_2 at different applied potentials on CN

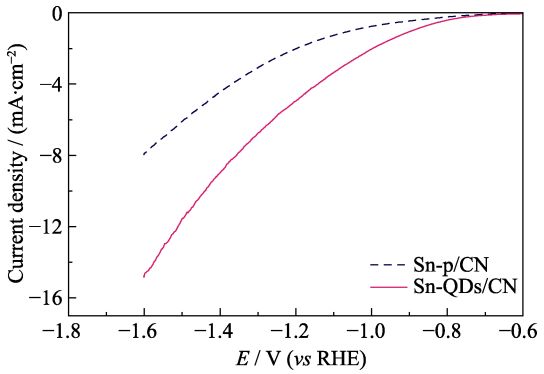

Fig. S5　LSV curves of Sn-p/CN and Sn-QDs/CN in CO_2-saturated 0.1 mol·L^{-1} $KHCO_3$ electrolyte at a scan rate of 30 mV·s^{-1}

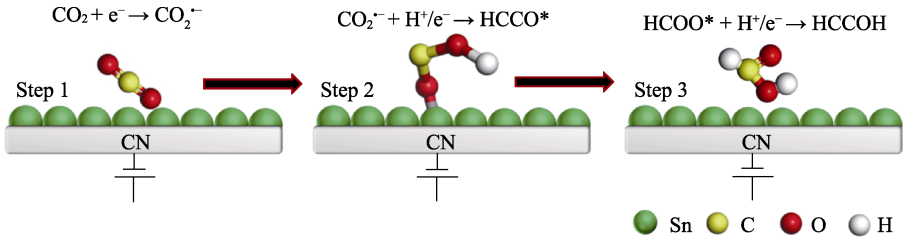

Fig. S6　Proposed possible reaction pathway of CO_2-to-HCOOH conversion on Sn-QDs/CN

References:

[1] LEI F C, SUN Y F, XU J Q, *et al*. Metallic tin quantum sheets confined in graphene toward high-efficiency carbon dioxide electroreduction. *Nature Communications*, 2016, **7:** 12697.

[2] ZHANG S, KANG P, J. MEYER T. Nanostructured tin catalysts for selective electrochemical reduction of carbon dioxide to formate, *Journal of the American Chemical Society*, 2014, **136:** 1734–1737.

[3] LIANG C L, KIM B, YANG S Z, *et al*. High efficiency electrochemical reduction of CO_2 beyond the two-electron transfer pathway on grain boundary rich ultra-small SnO_2 nanoparticles. *Journal of Materials Chemistry A*, 2018, **6:** 10313–10319.

[4] WANG Y, ZHOU J, LV W X, *et al*. Electrochemical reduction of CO_2 to formate catalyzed by electroplated tin coating on copper foam. *Applied Surface Science*, 2016, **362:** 394–398.

[5] WU J J, P. SHARMA P, HARRIS B H, *et al*. Electrochemical reduction of carbon dioxide: IV dependence of the Faradaic efficiency and current density on the microstructure and thickness of tin electrode. *Journal of Power Sources*, 2014, **258:** 189–194.

[6] BEJTKA K, ZENG J Q, SACCO A, *et al*. Chainlike mesoporous SnO_2 as a well-performing catalyst for electrochemical CO_2 reduction. *ACS Applied Energy Matericals*, 2019, **2:** 3081–3091.

[7] ZHANG B H, SUN L Z, WANG Y Q, *et al*. Well-dispersed SnO_2 nanocrystals on N-doped carbon nanowires as efficient electrocatalysts for carbon dioxide reduction. *Journal of Energy Chemistry*, 2020, **41:** 7–14.

[8] ZHANG B H, GUO Z H, ZUO Z, *et al*. The ensemble effect of nitrogen doping and ultrasmall SnO_2 nanocrystals on graphene sheets for efficient electroreduction of carbon dioxide. *Applied Catalysis B: Environmental*, 2018, **239:** 441–449.

[9] HE Y H, JIANG W J, ZHANG W J, *et al*. Pore-structure-directed CO_2 electroreduction to formate on SnO_2/C catalysts. *Journal of Materials Chemistry A*, 2019, **7:** 18428–18433.

[10] FU Y Y, WANG T T, ZHENG W Z, *et al*. Nanoconfined tin oxide within N-doped nanocarbon supported on electrochemically exfoliated graphene for efficient electroreduction of CO_2 to formate and C_1 products. *ACS Applied Materials & Interfaces*, 2020, **12:** 16178–16185.

[11] GU J, HEROGUEL F, LUTERBACHER J, *et al*. Densely packed, ultra small SnO nanoparticles for enhanced activity and selectivity in electrochemical CO_2 reduction. *Angewandte Chemie International Edition*, 2018, **57:** 2943–2947.